Organic Electronics 51 (2017) 173–179

Contents lists available at ScienceDirect

Organic Electronics

journal homepage: www.elsevier.com/locate/orgel

Suppression of efficiency roll-off in TADF-OLEDs using Ag-island nanostructures with localized surface plasmon resonance effect

Yue Yu [a], Lin Ma [a], Dongdong Wang [c], Huixin Zhou [a, **], Bo Yao [a], Zhaoxin Wu [b, *]

[a] School of Physics and Optoelectronic Engineering, Xidian University, Xi'an, 710071, People's Republic of China
[b] Key Laboratory of Photonics Technology for Information, Department of Electronic Science and Technology, School of Electronic and Information Engineering, Xi'an Jiaotong University, Xi'an, 710049, People's Republic of China
[c] Department of Chemistry, School of Science, Xi'an Jiaotong University, Xi'an, 710049, People's Republic of China

ARTICLE INFO

Article history:
Received 16 June 2017
Received in revised form
21 July 2017
Accepted 31 July 2017
Available online 3 August 2017

Keywords:
Thermally activated delayed fluorescence
Efficiency roll-off
Localized surface plasmon resonance
Ag-island nanostructures
Excited state

ABSTRACT

Organic light-emitting diodes (OLEDs) based on thermally activated delayed fluorescence (TADF) have emerged as promising alternatives to phosphorescent OLEDs for harvesting both singlet and triplet excitons. However, the development of TADF-OLEDs meets a thorny problem of serious efficiency roll-off at high luminance. Here, we demonstrate an approach to suppress the efficiency roll-off characteristics in TADF-OLEDs by localized surface plasmon resonance (LSPR) effect of easy-fabricated Ag-island nanostructures. Compared with the common TADF-OLEDs at a high current density of 100 mA cm^{-2}, the efficiency roll-off ratio of the TADF-OLEDs with Ag-island nanostructures decreases from 49.75% to 35.76% significantly, and the maximum current efficiency is increased by 10.5%. The performance enhancement is mainly attributed to the coupling between excitons and localized surface plasmons (LSPs), which could alter the excited state kinetic characteristics of TADF molecules.

1. Introduction

With the advantages of high luminous efficiency, access to flexible panels and facile color temperature tuning, organic light-emitting diodes (OLEDs) are a promising alternative to traditional inorganic light-emitting diodes (LEDs) for the revolutionary applications of future lighting sources [1–4]. Recently, fluorescent OLEDs based on thermally activated delayed fluorescence (TADF) materials without any expensive and non-renewable heavy-metal complexes have attracted tremendous attention as a promising approach for simultaneously obtaining high luminous efficiency, low cost and stability [5–9]. However, TADF-OLEDs suffer from serious efficiency reduction by a large margin at high current and brightness, which is called efficiency roll-off effect. Except for triplet-triplet annihilation originating from the long lifetime of triplet excited state (T_1), high singlet excited state (S_1) density due to reverse intersystem crossing (RISC) process generates singlet-triplet quenching [10], and the two superimposed factors make efficiency roll-off reduction challenging for practical lighting application. To address the efficiency roll-off issue in TADF-OLEDs, methods based on molecular structure design have been proposed including shortening excited state lifetime of TADF material by enlarging RISC rate and tuning the carrier balance using randomly oriented host molecules [11–15].

As localized surface plasmon resonance (LSPR) effect of metallic nanostructure could result large enhancement of the local electromagnetic fields [16–18], it has aroused considerable attention to improve the performance of optoelectronic devices, including OLEDs and organic solar cells [19–23]. According to Purcell effect, the coupling between excitons and surface plasmons (SPs) affects the kinetic characteristics of nearby molecules, accelerating the spontaneous emission rate of the system and creating a new channel for emission [24–27]. Although some research works have been done for emission enhancement of conventional fluorescence and phosphorescent OLEDs using metallic nanostructure [26–29], LSPR effect of metallic nanostructure, to our knowledge, has not been used to improve the performance, especially suppress efficiency roll-off characteristics in TADF-OLEDs. In this paper, we introduce Ag-island nanostructure in TADF-OLEDs by annealing of ultrathin Ag film, modulate the LSPR wavelength of Ag-island nanostructure to realize the superior effect in suppressing efficiency roll-off in TADF-OLEDs, and investigate the influence on

* Corresponding author.
** Corresponding author.
E-mail address: zhaoxinwu@mail.xjtu.edu.cn (Z. Wu).

http://dx.doi.org/10.1016/j.orgel.2017.07.053
1566-1199/

excited state kinetic characteristics of TADF molecule in the presence of Ag-island nanostructure with LSPR effect.

2. Experimental methods

2.1. Fabrication and characterization of Ag-island nanostructures

Fig. 1 shows the schematic of the preparation process for size-tunable Ag-island nanostructure. First, an ultrathin Ag film was deposited under high vacuum by thermal evaporation at a deposition rate of 0.02 nm/s on a cleaned and preprocessed glass substrate precoated with transparent and conductive indium tin oxide (ITO). Second, the ultrathin Ag film was annealed at 200 °C in vacuum for 30 min to obtain Ag-island nanostructure. After that, a 40-nm-thick 4,4′,4″-tris[2-naphthyl(phenyl)amino] triphenylamine (2T-NATA) hole injection layer was spin-coated from chlorobenzene solution at a concentration of 14 mg/ml and a speed of 1000 rpm, then baked at 80 °C in vacuum for 30 min to fill the gaps appropriately and make the 2T-NATA@Ag-island composite layer planarization.

Fig. 2 illustrates the surface morphology of ultrathin Ag films, Ag-island nanostructures, and 2T-NATA@Ag-island composite films by atomic force microscopy (AFM). As shown in Fig. 2(a)-(c), ultrathin Ag film was deposited to substantial thickness of 0.5, 1, and 3 nm, respectively. It can be clearly seen from Fig. 2(d)-(f) that, after annealing at 200 °C in vacuum for 30 min, these ultrathin Ag films exerts significant aggregation to form Ag-island nanostructure, and with the increase in thickness of ultrathin Ag film, the size of Ag-island grows gradually. Fig. 2(g) and (h) are AFM images of annealed 2T-NATA@Ag-island composite films, of which 2T-NATA layers were spin-coated at a speed of 2000 rpm and 1000 rpm on 1-nm-thick Ag film after annealing, respectively. According to the AFM images, a 40-nm-thick 2T-NATA layer spin-coated at a speed of 1000 rpm in Fig. 2(h) can appropriately cover Ag-island nanostructure and make surface planarization, while in Fig. 2(g) a portion of Ag-island nanostructure was exposed without covering due to thinner 2T-NATA layer.

The UV–vis absorption spectra of ultrathin Ag films without annealing and Ag-island nanostructures after annealing at 200 °C in vacuum for 30 min, as well as the photoluminescence (PL) spectra of the 15 nm-thick emitting layer with 5 wt% 4CzIPN emitter doped in CBP host are shown in Fig. 3. Due to the significant aggregation after annealing, the UV–vis absorption spectra of Ag-island nanostructures in Fig. 3(b) exhibited obvious bathochromic-shifts and clearer resonance peaks, and the resonance wavelength could be further controlled to the size of Ag-island by change the thickness of ultrathin Ag film. In addition, the UV–vis absorption spectra of 1 nm-thick Ag film after annealing was well-matched with the PL spectra of 4CzIPN emitter, as shown in Fig. 3(b). It is reported that LSPR will be efficiently excited when the degree of wavelength matching between the absorption spectra of metal nanostructure and PL spectra of luminescent molecule is high [22,30], so we used Ag-island nanostructure from annealing of 1 nm-thick Ag film in the fabrication and research of TADF-OLEDs.

2.2. OLED fabrication and characterizations

TADF-OLEDs were fabricated onto a cleaned glass substrate precoated with transparent and conductive indium tin oxide (ITO) by thermal evaporation process at a pressure of 1×10^{-4} Pa without vacuum break. Prior to organic layer deposition, ITO substrates were pretreated under UV-ozone flux for 10 min to increase its work function, following degreasing in acetone and isopropyl alcohol (IPA). The thickness of the films was determined by a quartz-crystal sensor. Active area of devices was 3×4 mm^2 for all the samples studied in this work. The current density-voltage-luminance-efficiency (*J-V-L-η*) characteristics of the devices were measured with a Keithley 2602 and Source Meter. All the measurements were carried out at room temperature under ambient conditions. PL and UV–vis absorption spectra were recorded by a Horiba Jobin Yvon Fluoromax-4 spectrophotometer and a Hitachi UV 3010 spectrophotometer, respectively. The PR650 spectrophotometer and fiber optic spectrometer is utilized to measure the

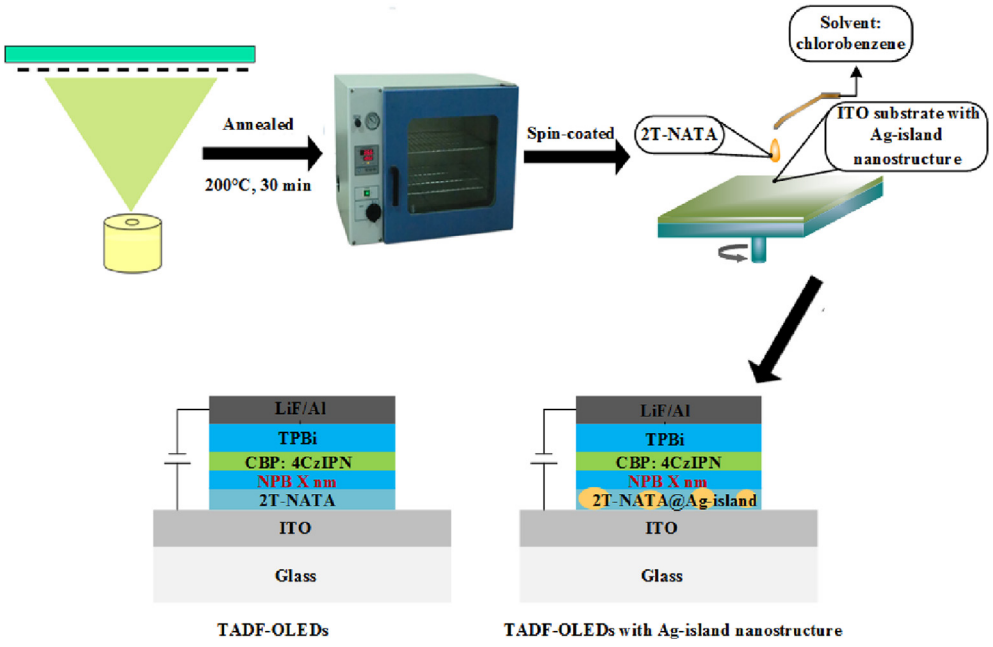

Fig. 1. Schematic of the preparation process for TADF-OLEDs with Ag-island nanostructure.

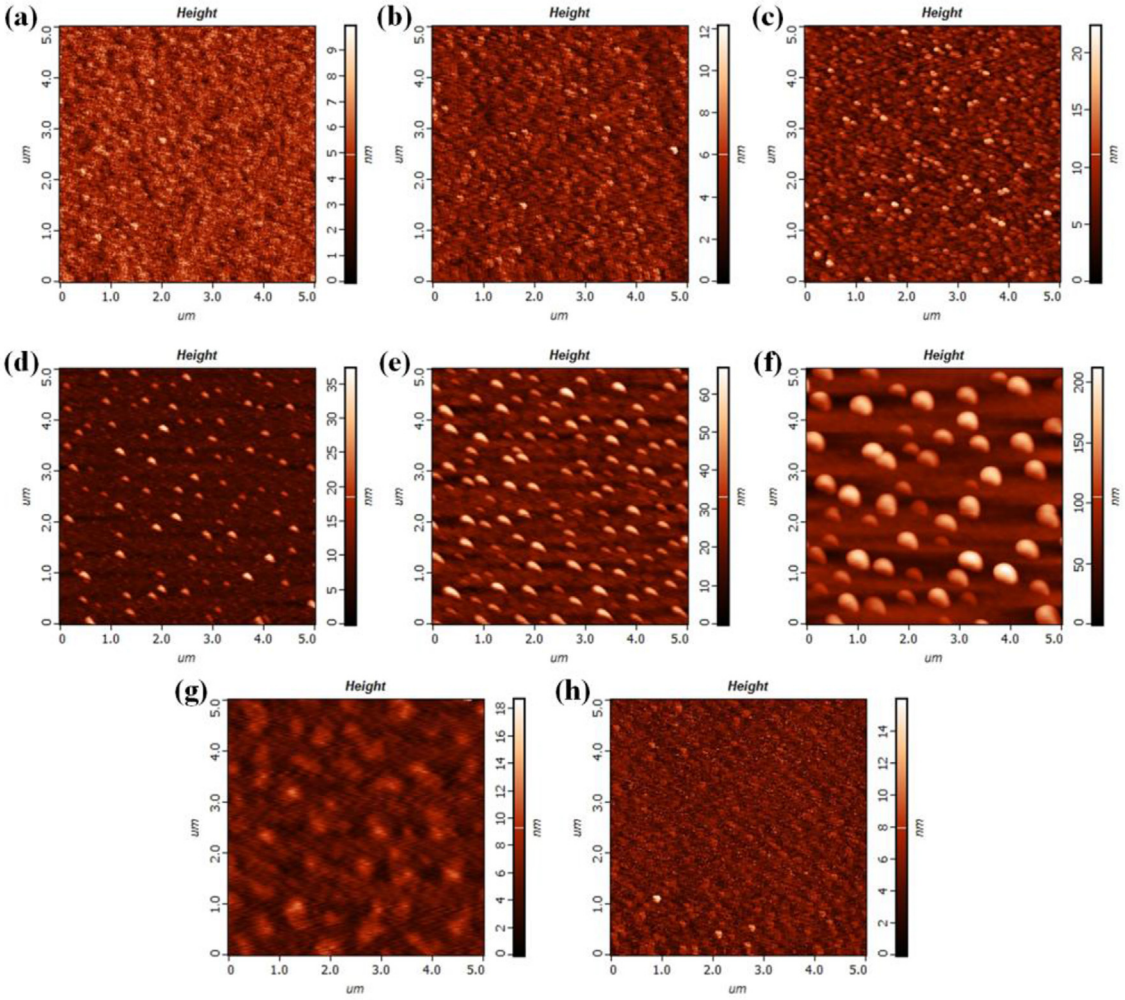

Fig. 2. The AFM images of ultrathin Ag films for (a) 0.5 nm, (b) 1 nm, (c) 3 nm before annealing. The AFM images of Ag-island nanostructures for (d) 0.5 nm-thick, (e) 1 nm-thick, (f) 3 nm-thick Ag film after annealing at 200 °C for 30 min. The AFM images of annealed 2T-NATA@Ag-island composite films for (g) 2T-NATA layer spin-coated at 2000 rpm on 1-nm-thick Ag film after annealing, (h) 2T-NATA layer spin-coated at 1000 rpm on 1-nm-thick Ag film after annealing.

electroluminescent (EL) spectra.

For TADF-OLEDs fabrication, the stacked organic layer of [4,4′-bis[*N*-(1-naphthyl)-*N*-phenyl-amino]biphenyl (NPB) (x nm)/4,4′-bis(*N*-carbazolyl)biphenyl (CBP): 1,2,3,5-tetrakis(carbazol-9-yl)-4,6-dicyanobenzene (4CzIPN) (5 wt%) (15 nm)/1,3,5-tris(1-phenyl-1*H*-benzimidazol-2-yl)benzene (TPBi) (55 nm)] and the [LiF (1 nm)/Al (70 nm)] cathode layer were successively deposited by vacuum deposition on the 2T-NATA film. The well known TADF material 4CzIPN was doped in CBP host to form the emitting layer with the optimal doping concentration of 5 wt% [6]. NPB was used as hole transporting layer and spacer, and TPBi was utilized as electron transporting layer and exciton blocking layer. To demonstrate the influence of Ag-island nanostructures on TADF-OLEDs, two kinds of devices with and without Ag-island nanostructures were prepared. After optimizing parameters, the configuration details of the two kinds of devices are confirmed as follows:

Device type A: Glass/ITO/2T-NATA (40 nm)@Ag-island/NPB (x nm)/CBP: 4CzIPN (5 wt%) (15 nm)/TPBi (55 nm)/LiF (1 nm)/Al.
Device type B: Glass/ITO/2T-NATA (40 nm)/NPB (x nm)/CBP: 4CzIPN (5 wt%) (15 nm)/TPBi (55 nm)/LiF (1 nm)/Al.

And for x = 0, 5, 15, 25, the devices were defined as device A1, A2, A3, A4 or device B1, B2, B3, B4, respectively.

3. Results and discussions

Fig. 4 shows the current density-voltage-luminance-efficiency (*J-V-L-η*) characteristics of the devices. The key device performance parameters are summarized in Table 1. As shown in Fig. 4(a), current density decreases very slightly with the introduction of Ag-island nanostructures, and we think it may be caused by the hole-trapping effect of Ag-island. The current efficiency-current density characteristics of the devices are shown in Fig. 4(c), compared to device B1, B2, B3, B4 without Ag-island nanostructures, current efficiency of device A1, A2, A3, A4 has improved for −14.0%, 10.5%, 5.6% and 1.9%, respectively. Since fluorescence quenching takes place due to short distance from TADF emitting molecules to the metal surface, the current efficiency of device A1 decreases compared to device B1. It has been reported that LSPR decays exponentially with the distance increase from SPs to emitting molecules [26,31]. For device A2 and A3, the current efficiency has been enhanced obviously in comparison to the reference device, because coupling between the excitons of TADF molecules and SPs occurs on account of efficient energy transfer between emitting

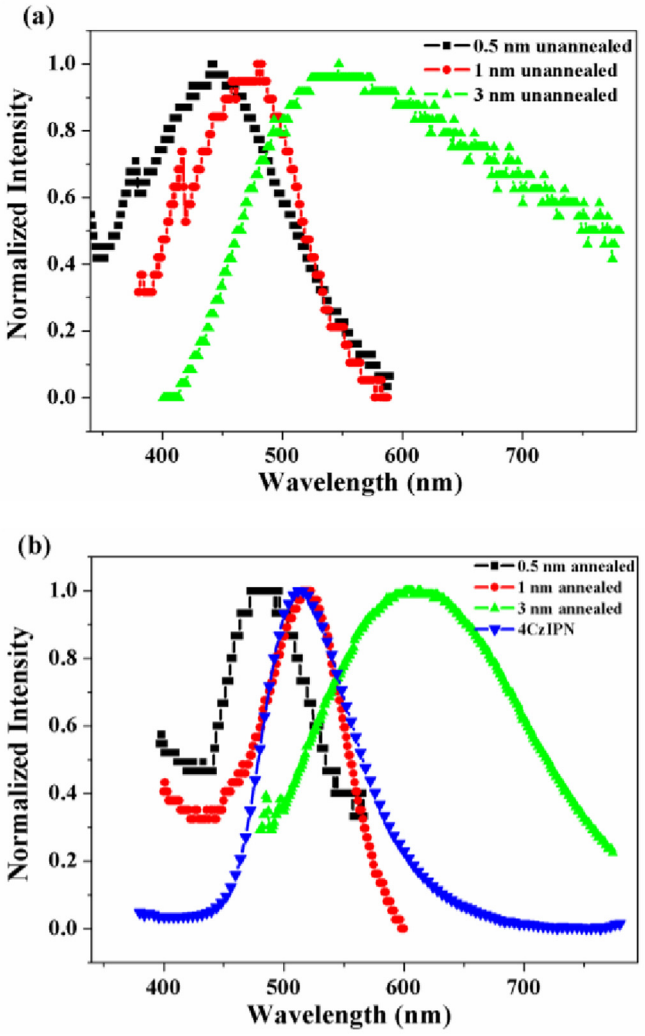

Fig. 3. (a) UV–vis absorption spectra of ultrathin Ag films before annealing. (b) UV–vis absorption spectra of Ag-island nanostructures after annealing at 200 °C for 30 min and PL spectra of a 15 nm-thick film with 5 wt% 4CzIPN emitted doped in CBP host.

molecules and SPs, creating an alternate channel for radiation [27]. But, further increase the thickness of NPB spacer layer in device A4 did not improve the current efficiency much due to the lack of exciton-SP coupling.

To investigate the effect of Ag-island nanostructures on efficiency roll-off in TADF-OLEDs, the efficiency roll-off ratio is determined by $(\eta_{max}-\eta)/\eta_{max}$, where η_{max} and η are the maximum current efficiency and the current efficiency at an arbitrary current density or brightness. For instance, at a high current density of 100 mA cm^{-2}, the efficiency roll-off ratio was 28.11%, 45.86%, 35.76%, 49.75%, 42.13%, 48.24%, 49.88% and 51.13% for device A1, B1, A2, B2, A3, B3, A4 and B4, respectively. Although the current efficiency of device A1 is lower than that of device B1, the efficiency roll-off ratio of device A1 is the smallest of all the TADF-OLEDs fabricated, indicating that exciton-SP coupling is most effective due to efficient energy transfer process. Besides, the efficiency roll-off characteristics become much more serious with the thickness of NPB spacer layer of device A1-A4 layer increased. When the thickness of NPB spacer layer in device A4 was increased to 25 nm, the energy transfer process between excitons and SPs became invalid, thus leading to almost the same device performance of device A4 and B4. Fig. 5 shows the current efficiency-current density curves and roll-off characteristics of device 2A and 2B. In general, device 2A with a 5 nm-thick NPB spacer layer exhibits the most remarkable performance improvement compared to device B2 due to the strong exciton-SP coupling by introducing Ag-island nanostructures.

The normalized EL spectra of device 2A and 2B at current density of 100 mA cm^{-2} are shown in Fig. 6(a). Both device 2A and 2B show almost the same bright green emission with a vibronic peak around 528 nm, which is the characteristic of the emission from 4CzIPN TADF dopant [6], and the slightly narrowing in EL spectra of device 2A compared to device B2 may be caused by Ag-island nanostructures due to weakly microcavity effect [32]. Furthermore, for the angular-dependent emission pattern, the device is fixed on a rotational stage, and the EL intensity and spectrum are then measured with a calibrated fiber optical spectrometer at every ten degrees from 0° to 80°. Fig. 6(b) shows the angular dependence of the emission for the TADF-OLEDs with (device 2A) and without (device 2B) Ag-island nanostructures as well as the ideal Lambertian curve for comparison. Both device 2A and 2B exhibit almost Lambertian emission pattern, indicating the great potential for the light application of TADF-OLEDs with Ag-island nanostructures.

To further verify the exciton-SP coupling mechanism, we fabricated two samples to measure the room-temperature time-resolved PL traces. The configuration details are shown as follows:

Sample A: Glass/ITO/2T-NATA (40 nm)@Ag-island/NPB (5 nm)/CBP: 4CzIPN (5 wt%) (15 nm).
Sample B: Glass/ITO/2T-NATA (40 nm)/NPB (5 nm)/CBP: 4CzIPN (5 wt%) (15 nm).

It has been reported that exciton-SP coupling is faster than spontaneous emission of excitons, and the excited state lifetime of the excitonic system should be decreased, thereby altering the spontaneous emission rate of system [33,34]. Fig. 7 illustrates PL decay curves for emission of 4CzIPN at room temperature in sample A and B. The prompt component observed is attributed to the fluorescence, and the delayed component as a long tail is assigned to TADF occurring by means of RISC. As shown in Fig. 7, the lifetime of fluorescence component (τ_F) decreases from 17.9 ns (sample B) to 16.7 ns (sample A), and lifetime of TADF component (τ_{TADF}) also significant reduces from 4.8 μs (sample B) to 4.4 μs (sample A), indicating that effective exciton-SP coupling could take place. Fig. 8 shows excitons radiation phenomena in TADF-OLEDs. As exciton-SP coupling would affect the kinetic characteristics of nearby molecules [35,36], on one hand, the coupling between excitons and SPs would enhance radiative decay rate of the excitonic system, reduce τ_F of S_1 and decrease excitons density, on the other, according to principle of dynamics, the reduction of S_1 density could accelerate RISC process of $T_1 \rightarrow S_1$, thus further decreasing the density of T_1 and reducing τ_{TADF} of TADF. The reduction of both τ_F and τ_{TADF} in PL decay measurement has confirmed the explanation above, and performance improvements including marked efficiency enhancement and significant efficiency roll-off suppression can be achieved owing to the acceleration of spontaneous radiation and the decrease of T_1 density by introducing Ag-island nanostructures in TADF-OLEDs.

4. Conclusions

In conclusion, we introduced easy-fabricated Ag-island nanostructures into TADF-OLEDs and achieved significant efficiency enhancement and efficiency roll-off suppression. Compared with the common green TADF-OLEDs based on 4CzIPN emitter at a high

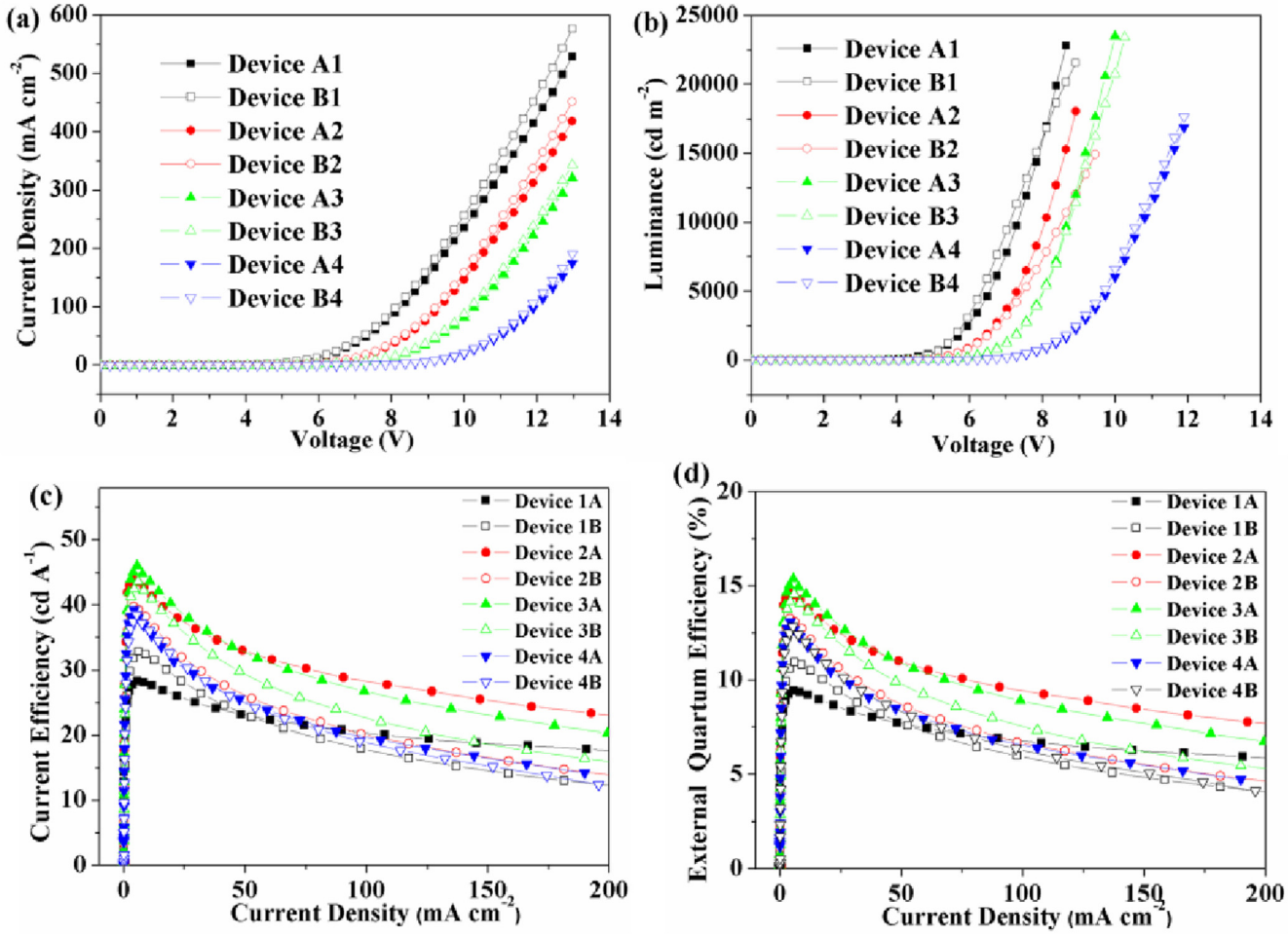

Fig. 4. (a) Current density-voltage characteristics. (b) Brightness-voltage characteristics. (c) Current efficiency-current density characteristics. (d) External quantum efficiency (EQE)-current density characteristics of device A1–A4 and device B1–B4.

current density of 100 mA cm^{-2}, our modified TADF device with Ag-island nanostructures exhibits a reduction in efficiency roll-off ratio from 49.75% to 35.76%, and the current efficiency is enhanced by 10.5%. The performance enhancement is mainly attributed to the exciton-SP coupling between 4CzIPN molecules and SPs. Our work provides a new approach to suppress the efficiency roll-off characteristics in highly efficient TADF-OLEDs, which will benefit practical display and lighting applications of TADF-OLEDs.

Table 1
EL performance the devices A1–A4 and B1–B4.

Device	λ_{max}^{EL} [a] (nm)	V_{on} [b] (V)	B_{max} [c] (cd m^{-2})	η_{ext} [d] (%)	η_c [d] (cd A^{-1})	Roll-off ratio[e/f/g] (%)	CIE[a] (x, y)
A1	528	2.9	23010	9.43 ± 0.7	28.28 ± 2.0	28.11/12.44/22.37	(0.336, 0.570)
B1	528	2.8	23898	10.97 ± 0.8	32.88 ± 2.4	45.86/19.81/35.62	(0.340, 0.566)
A2	528	3.1	23904	14.66 ± 1.1	43.96 ± 3.3	35.76/16.77/30.11	(0.338, 0.568)
B2	528	3.0	22098	13.27 ± 1.0	39.78 ± 3.0	49.75/22.98/41.29	(0.337, 0.570)
A3	530	3.2	24983	15.36 ± 1.2	46.09 ± 3.6	42.13/19.39/34.79	(0.336, 0.568)
B3	530	3.1	23998	14.55 ± 1.1	43.64 ± 3.3	48.24/21.71/39.22	(0.338, 0.567)
A4	532	3.5	23076	13.07 ± 0.8	39.21 ± 2.4	49.88/23.29/41.80	(0.337, 0.569)
B4	532	3.4	22896	12.82 ± 0.8	38.47 ± 2.3	51.13/23.41/42.17	(0.338, 0.568)

[a] Values collected at current density of 100 mA cm^{-2}.
[b] Turn-on voltage at 1 cd m^{-2}.
[c] Maximum brightness.
[d] Values collected at a peak efficiency.
[e] Roll-off ratio at a current density of 100 mA cm^{-2}.
[f] Roll-off ratio at a luminance of 1000 cd m^{-2}.
[g] Roll-off ratio at a luminance of 10000 cd m^{-2}.

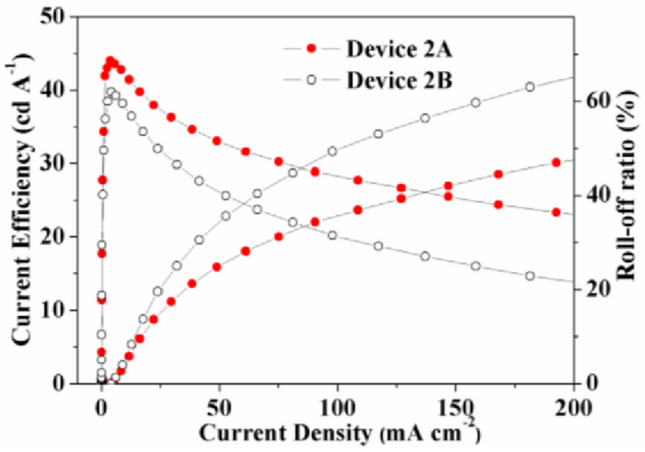

Fig. 5. Current efficiency-current density curves and roll-off characteristics of device 2A and 2B.

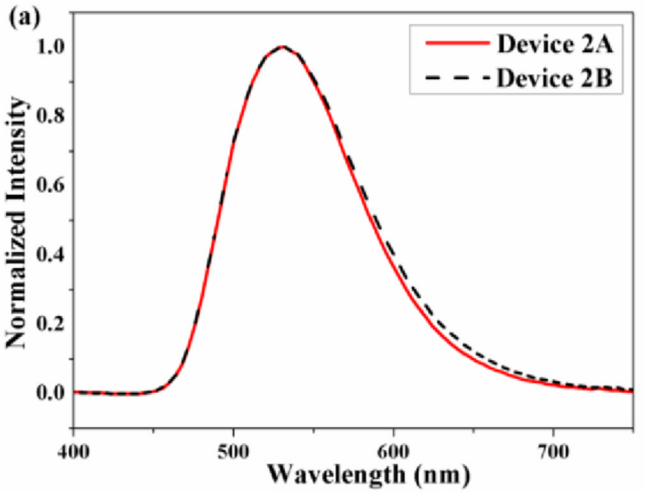

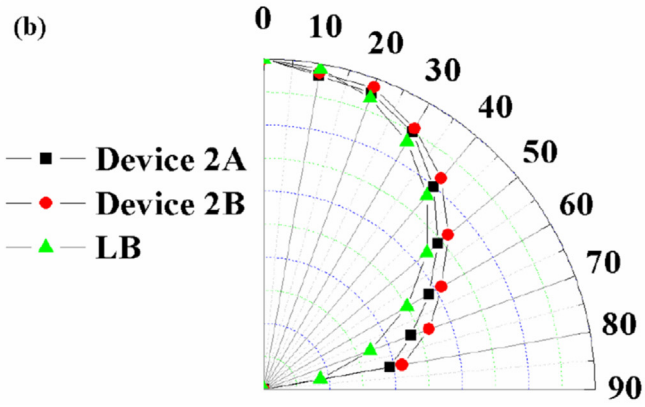

Fig. 6. (a) EL spectra of device 2A and 2B at 8 V. (b) Emission pattern of device 2A, 2B (normalized to the intensity at 0°), and the lambertian (LB) pattern is used as reference.

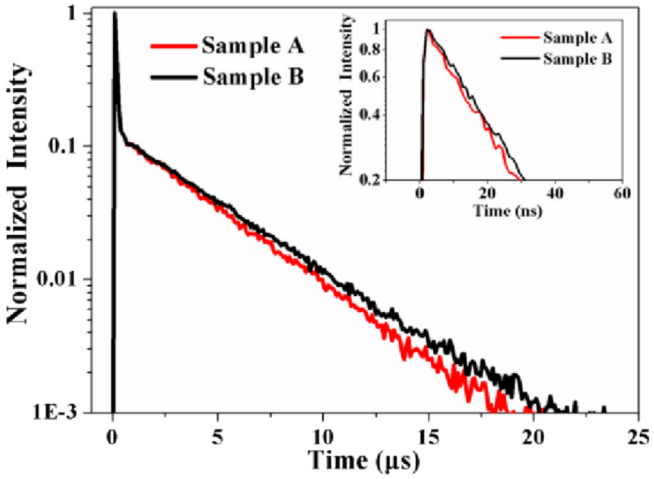

Fig. 7. PL decay curves of sample A and B excited at a wavelength of 350 nm.

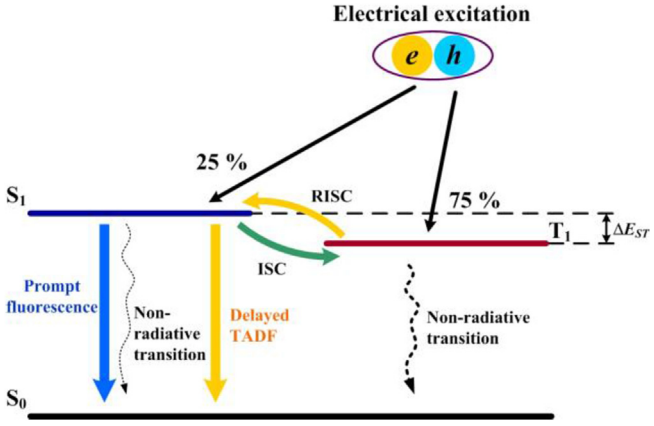

Fig. 8. Singlet and triplet excitons radiation phenomena in TADF-OLEDs.

Acknowledgements

This work was financially supported by Key Research Program of China (2016YFB0400702) and the Fundamental Research Funds for the Central Universities.

References

[1] C.W. Tang, S.A. VanSlyke, Appl. Phys. Lett. 51 (1987) 913.
[2] Y. Sun, N.C. Giebink, H. Kanno, B. Ma, M.E. Thompson, S.R. Forrest, Nature 440 (2006) 908.
[3] S. Reineke, F. Lindner, G. Schwartz, N. Seidler, K. Walzer, B. Sussem, K. Leo, Nature 459 (2009) 234.
[4] M.G. Helander, Z. Wang, J. Qiu, M.T. Greiner, D.P. Puzzo, Z. Liu, Z. Lu, Science 332 (2011) 944.
[5] M. Endo, A. Ogasawara, D. Takahashi, Y. Yokoyama, C. Kato, Adachi, Adv. Mater. 21 (2009) 4802.
[6] H. Uoyama, K. Goushi, K. Shizu, H. Nomura, C. Adachi, Nature 492 (2012) 234.
[7] S. Hirata, Y. Sakai, K. Masui, H. Tanaka, S.Y. Lee, H. Nomura, N. Nakamura, M. Yasumatsu, H. Nakanotani, Q. Zhang, K. Shizu, H. Miyazaki, C. Adachi, Nat. Mater. 14 (2015) 330.
[8] Q. Zhang, B. Li, S. Huang, H. Nomura, H. Tanaka, C. Adachi, Nat. Photonics 8 (2014) 326.
[9] D. Zhang, P. Wei, D. Zhang, L. Duan, ACS Appl. Mater. Interfaces 9 (2017) 19040.
[10] K. Masui, H. Nakanotani, C. Adachi, Org. Electron 14 (2013) 2721.

[11] D. Zhang, C. Zhao, Y. Zhang, X. Song, P. Wei, M. Cai, L. Duan, ACS Appl. Mater. Interfaces 9 (2017) 4769.
[12] M. Inouea, T. Sereviˇcius, H. Nakanotani, K. Yoshida, T. Matsushima, S. Juršˇenas, C. Adachi, Chem. Phys. Lett. 16 (2016) 62.
[13] X. Cai, X. Li, G. Xie, Z. He, K. Gao, K. Liu, D. Chen, Y. Cao, S. Su, Chem. Sci. 7 (2016) 4264.
[14] T. Komino, H. Nomura, T. Koyanagi, C. Adachi, Chem. Mater. 25 (2013) 3038.
[15] S. Wang, Y. Zhang, W. Chen, J. Wei, Y. Liu, Y. Wang, Chem. Commun. 51 (2015) 11972.
[16] K.L. Kelly, E. Coronado, L.L. Zhao, G.C. Schatz, J. Phys. Chem. B 107 (2003) 668.
[17] E. Hutter, J.H. Fendler, Adv. Mater. 16 (2004) 1685.
[18] W.L. Barnes, A. Dereux, T.W. Ebbesen, Nature 424 (2003) 824.
[19] M.K. Kwon, J.Y. Kim, B.H. Kim, I.K. Park, C.Y. Cho, C.C. Byeon, S.J. Park, Adv. Mater. 20 (2008) 1253.
[20] F. Chen, J. Wu, C.L. Lee, Y. Hong, C.H. Kuo, M. Huang, Appl. Phys. Lett. 95 (2009) 013303.
[21] K. Togashi, S. Nomura, N. Yokoyama, T. Yasuda, C. Adachi, J. Mater. Chem. 22 (2012) 20689.
[22] X. Liu, D. Li, X. Sun, Z. Li, H. Song, H. Jiang, Y. Chen, Sci. Rep. 5 (2015) 12555.
[23] J. Hu, Y. Yu, B. Jiao, S. Ning, H. Dong, X. Hou, Z. Zhang, Z. Wu, Org. Electron 31 (2016) 234.
[24] S.T. Kochuveedu, D.H. Kim, Nanoscale 6 (2014) 4966.
[25] E. Fort, S. Grésillon, J. Phys. D. Appl. Phys. 41 (2008) 013001.
[26] D. Zhang, R. Wang, Y. Ma, H. Wei, Q. Ou, Q. Wang, L. Zhou, S.T. Lee, Y. Li, J. Tang, Org. Electron 15 (2014) 961.
[27] A. Kumar, R. Srivastava, P. Tyagi, D.S. Mehta, M.N. Kamalasanan, Org. Electron 13 (2012) 159.
[28] W. Ji, H. Zhao, H. Yang, Org. Electron 22 (2015) 154.
[29] Y. Zhao, F. Yun, Y. Huang, Z. Wu, Y. Li, B. Jiao, L. Feng, S. Li, W. Ding, Y. Zhang, Appl. Phys. Lett. 109 (2016) 013303.
[30] H. Lee, L.W. Jang, A.Y. Polyakov, Nano Energy 13 (2015) 140.
[31] W. Gaynor, S. Hofmann, M.G. Christoforo, C. Sachse, S. Mehra, A. Salleo, M.D. Mcgehee, M.C. Gather, B. Lüssem, L.M. Meskamp, P. Peumans, K. Leo, Adv. Mater. 25 (2013) 4006.
[32] R. Meerheim, R. Nitsche, K. Leo, Appl. Phys. Lett. 93 (2008) 043310.
[33] A. Kumar, P. Tyagi, R. Srivastava, D.S. Mehta, M.N. Kamalasanan, Appl. Phys. Lett. 102 (2013) 203304.
[34] Y. Xiao, J. Yang, P. Cheng, J. Zhu, Z. Xu, Y. Deng, S.T. Lee, Y. Li, J. Tang, Appl. Phys. Lett. 100 (2012) 013308.
[35] F. Tam, G.P. Goodrich, B.R. Johnson, N.J. Halas, Nano Lett. 7 (2007) 496.
[36] A. Kinkhabwala, Z. Yu, S. Fan, Y. Avlasevich, K. Müllen, W.E. Moerner, Nat. Photonics 3 (2009) 654.